Inorganic Chemistry

FORUM ARTICLE

pubs.acs.org/IC

Study of Molybdenum(4+) Quinoxalyldithiolenes as Models for the Noninnocent Pyranopterin in the Molybdenum Cofactor

Kelly G. Matz,[†] Regina P. Mtei,[‡] Rebecca Rothstein,[†] Martin L. Kirk,*[,‡] and Sharon J. Nieter Burgmayer*[,†]

[†]Department of Chemistry, Bryn Mawr College, Bryn Mawr, Pennsylvania 19010, United States

[‡]Department of Chemistry and Chemical Biology, The University of New Mexico, Albuquerque, New Mexico 87131-0001, United States

ABSTRACT:

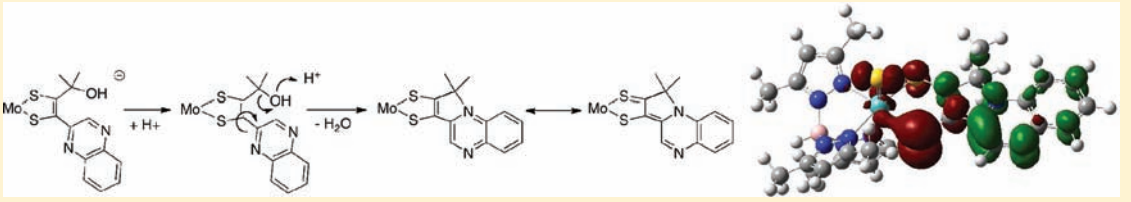

A model system for the molybdenum cofactor has been developed that illustrates the noninnocent behavior of an N-heterocycle appended to a dithiolene chelate on molybdenum. The pyranopterin of the molybdenum cofactor is modeled by a quinoxalyldithiolene ligand (S_2BMOQO) formed from the reaction of molybdenum tetrasulfide and quinoxalylalkyne. The resulting complexes TEA[Tp*MoX(S_2BMOQO)] [**1**, X = S; **3**, X = O; TEA = tetraethylammonium; Tp* = hydrotris(3,5-dimethylpyrazolyl)-borate] undergo a dehydration-driven intramolecular cyclization within quinoxalyldithiolene, forming Tp*MoX(pyrrolo-S_2BMOQO) (**2**, X = S; **4**, X = O). **4** can be oxidized by one electron to produce the molybdenum(5+) complex **5**. In a preliminary report of this work, evidence from X-ray crystallography, electronic absorption and resonance Raman spectroscopies, and density functional theory (DFT) bonding calculations revealed that **4** possesses an unusual asymmetric dithiolene chelate with significant thione−thiolate character. The results described here provide a detailed description of the reaction conditions that lead to the formation of **4**. Data from cyclic voltammetry, additional DFT calculations, and several spectroscopic methods (IR, electronic absorption, resonance Raman, and electron paramagnetic resonance) have been used to characterize the properties of members in this suite of five Mo(S_2BMOQO) complexes and further substantiate the highly electron-withdrawing character of the pyrrolo-S_2BMOQO ligand in **2**, **4**, and **5**. This study of the unique noninnocent ligand S_2BMOQO provides examples of the roles that the N-heterocycle pterin can play as an essential part of the molybdenum cofactor. The versatile nature of a dithiolene appended by heterocycles may aid in modulating the redox processes of the molybdenum center during the course of enzyme catalysis.

INTRODUCTION

Metal complexes with dithiolene ligands were first investigated during the 1960s,[1] and because of their many unusual properties, they remain a focus of study 50 years later. Metal dithiolenes have significant roles in biological catalysis[2,3] and in materials research,[4−8] especially electronics and sensor applications.[9,10] Progress made in detailing the electronic structure of metal dithiolenes has been a vehicle to understanding their unusual properties. The highly covalent metal dithiolene unit possesses flexible redox behavior that facilitates intramolecular metal−ligand redox processes.[11] As such, dithiolene ligands exhibit "noninnocent" behavior and metal dithiolenes are among a limited number of inorganic systems that display extensive metal−ligand redox interplay, making them useful as key components of donor−acceptor molecules.[12,13] From a valence-bond perspective, dithiolene ligands can be viewed as existing somewhere between the extremes of the neutral dithione−dithiete and dianionic dithiolate ligand forms (Figure 1). This description is distinct from the formal oxidation state behavior observed for dioxolene ligand complexes, which display a well-behaved quinone−semiquinone−catecholate series, with discrete oxidation states being assigned to the ligand and metal.[14] The principal difference between dianionic and neutral dithiolene ligands is the number of π electrons present in the S−C═C−S backbone of the dithiolene. For the neutral dithiones, the S═C−C═S fragment possesses four π electrons, and for the dianionic form, there are six π electrons.

Our curiosity about molybdenum dithiolenes has led our query into their partnership with pterins in the pyranopterin molybdenum enzymes.[2] Pterins possess multiple redox states accessed through complicated redox processes and, like dithiolenes, have been shown to be noninnocent redox partners with metals.[15−19] For example, reduced pterins chelated to Mo at the O4 and N5 sites can generate three resonance structures where the electron density shifts from a deprotonated tetrahyropterin to the Mo atom, resulting in the three valence tautomeric structures of Scheme 1.[20]

The molybdenum pterin dithiolene structure found at the catalytic active site (Figure 2) within pyranopterin molybdenum

Received: April 16, 2011
Published: September 06, 2011

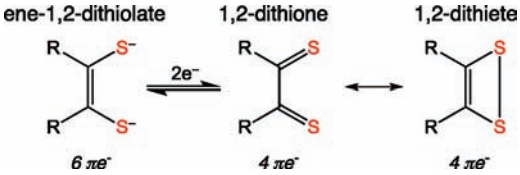

Figure 1. Valence-bond description of dithiolene ligand forms. Two-electron oxidation of the ene-1,2-dithiolate leads to oxidized forms described by 1,2-dithione and 1,2-dithiete Lewis structures.

Scheme 1. Three Valence Tautomeric Structures for Reduced Pterin Chelating Mo Illustrating: a Deprotonated Tetrahydropterin Coordinated to Molybdenum(6+) in A, a Neutral Trihydropterin Radical Coordinated to Molybdenum(5+) in B, and a Protonated Dihydropterin Coordinated to Molybdenum(4+) in C

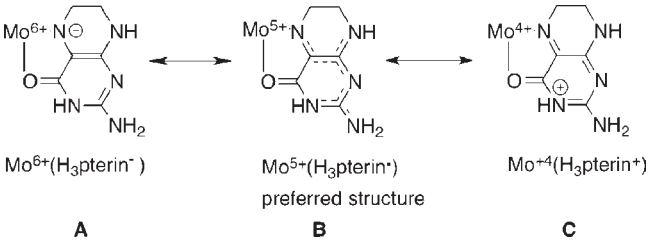

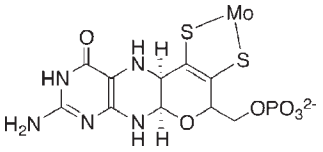

Figure 2. Pyranopterin dithiolene ligand in the molybdenum cofactor, Moco, the catalytic site in molybdenum enzymes.

enzymes creates the most redox-rich unit known in bioinorganic chemistry. The Mo atom participates in two-electron redox chemistry coupled to formal O-atom transfer, the dithiolene has the capability of two-electron oxidation to a dithione, and the pyranopterin unit can potentially participate in multielectron transfer. In addition, the redox chemistry of pterins is necessarily associated with proton transfer, presenting further opportunities for the protein to induce noninnocent behavior at the molybdenum cofactor controlled through hydrogen bonding between pyranopterin and nearby protein residues. Several groups have speculated on possible ways that the pyranopterin dithiolene ligand might be an active component of the catalytic reaction.[21−23] Possible roles include participation as an electronic conduit between the molybdenum center and other electron-transfer units in the protein and as a switch to adjust the molybdenum redox potential. Credence for these speculations has been provided by several recent X-ray structures that show that the pyran ring of the dithiolene ligand on Moco can exist in both the closed pyrano form and the open, noncyclized form.[24−26]

Because it is difficult to directly study the behavior of the pyranopterin dithiolene in Moco while bound within the protein, we have turned to small-molecule analogue studies to obtain such information. Our strategy for exploring the possibilities created by a molybdenum−pterin−dithiolene partnership has been to develop the reaction chemistry of pterin- and quinoxaline-substituted dithiolene complexes of molybdenum to serve as small-molecule analogues for studying the effects of these N-heterocycles on dithiolene properties.[27]

In a recent Communication, we reported the unusual electronic structure exhibited by an oxomolybdenum(4+) quinoxaline-substituted dithiolene complex, Tp*Mo^{4+}(O)(pyrrolo-S_2BMOQO) [Tp* is hydrotris(3,5-dimethylpyrazolyl)borate] containing a rare thiolate−thione ligand.[28] This compound exhibits a remarkable donor−acceptor character that affects the $Mo^{5+/4+}$ redox couple and beautifully illustrates the potentially noninnocent role of an N-heterocycle, such as pterin, in modulating molybdenum redox potentials during the course of pyranopterin molybdenum enzyme catalysis. Here we describe in more detail the synthesis, reaction chemistry, and properties of other members of the S_2BMOQO family of quinoxalyldithiolene complexes of molybdenum: TEA[Tp*Mo^{4+}(S)(S_2BMOQO)] (**1**), Tp*Mo^{4+}(S)-(pyrrolo-S_2BMOQO) (**2**), TEA[Tp*Mo^{4+}(O)(S_2BMOQO)] (**3**), Tp*Mo^{4+}(O)(pyrrolo-S_2BMOQO) (**4**), and [Tp*Mo^{5+}-(O)(pyrrolo-S_2BMOQO)]Cl (**5**).

EXPERIMENTAL SECTION

Materials and Methods. All syntheses were conducted under an anaerobic atmosphere using standard Schlenk techniques unless otherwise noted. Solvents were dried over activated molecular sieves overnight to remove residual water. 2-Chloroquinoxaline was purchased from Sigma-Aldrich and purified by sublimation using a McCarter vacuum apparatus. TEA[Tp*$Mo^0(CO)_3$] [Tp* = hydrotris(3,5-dimethylpyrazolyl)borate; TEA^+ = tetraethylammonium] was prepared following the method of Curtis and Shiu[29] and then thoroughly washed with methanol to remove residual water, ether, and hexanes before drying under vacuum. TEA[Tp*$Mo^{4+}S(S_4)$] was prepared by a slight adaptation of a previously reported procedure,[27] where activated 3 Å molecular sieves replace alumina. NMR spectra were obtained from a Bruker 300 MHz or Varian INOVA 500 MHz instrument. IR spectra were collected on a Perkin-Elmer model 2000 FT-IR spectrometer from samples prepared as KBr pellets. Electrospray ionization mass spectrometry (ESI-MS) spectra were obtained on a Waters Micromass ZQ. High resolution ESI-MS (HRESI-MS) spectra were obtained by Dr. Somogyi at the Mass Spectrometry Facility in the Department of Chemistry at the University of Arizona on an Ion Spec Fourier transform mass spectrometer. Samples for mass spectral analysis were dissolved in acetonitrile (ACN) under aerobic conditions and directly injected, bypassing the liquid chromatography column.

UV−vis data were obtained on a Beckman DU 800 spectrophotometer. Electrochemical analyses were performed using a BioAnalytical Systems CV50 system, using tetrabutylammonium perchlorate (TBAP) as the electrolyte in ACN, platinum working, and auxiliary electrodes and Ag/AgCl as the reference electrode. All potentials are referenced to an internal ferrocene potential (+0.40 V vs Ag/AgCl).

Synthesis. *2-(3-Butynyl-2-methyl-2-ol)quinoxaline (BMOQO).* Cl_2-$Pd(PPh_3)_2$ (0.1130 g, 0.1610 mmol) in triethylamine (100 mL) and dimethyl sulfoxide (DMSO; 40 mL) was stirred under nitrogen for 10 min. The solution was stirred for 10 min after each addition of the remaining reagents: copper iodide (0.0307 g, 0.1612 mmol), 2-chloroquinoxaline (2.240 g, 0.01360 mol), and 2-methyl-3-butyn-2-ol (1.3 mL, 0.01341 mol). Stirring 6 h at room temperature caused the triethylamine layer to become bright yellow, while the DMSO layer containing the catalysts and product turned dark brown. The reaction flask was briefly chilled at 4 °C (45 min) to freeze the brown DMSO layer. The triethylamine layer was decanted and discarded. Distilled water (100 mL) was added to the frozen DMSO layer, and the thawed mixture was poured into a separatory funnel. The organic layer was extracted with dichloromethane and washed three times with 30 mL portions

dx.doi.org/10.1021/ic200783a |Inorg. Chem. 2011, 50, 9804–9815

of distilled water, and the water layer was backextracted with three 30 mL portions of dichloromethane. The organic layers were combined and washed twice with 20 mL portions of saturated aqueous NaCl before they were dried over magnesium sulfate. After filtration to remove $MgSO_4$, the CH_2Cl_2 solution containing BMOQO was rotary evaporated to produce a light-brown solid, which was dried under vacuum overnight. A tan solid was obtained in 91% yield (2.624 g, 0.01232 mol). ^{1}H NMR ($CDCl_3$, ppm): δ 8.88 (1H, s, quin *H*3), 8.12−8.08 (2H, m, Ar*H*), 7.83−7.76 (2H, m, Ar*H*), 2.28 (1H, s, O*H*), 1.70 (6H, s, C−CH_3). ESI-MS (CH_3CN): *m*/*z* 212 ([M]$^-$).

*TEA[Tp*Mo^{4+}(S)(S_2BMOQO)]* (**1**). ACN (40 mL) was transferred to a flask containing TEA[Tp*Mo^{4+}(S)(S_4)] (0.2170 g, 0.3168 mmol) and BMOQO (0.0672 g, 0.3169 mmol). The reaction was stirred at room temperature for 4 h and then chilled in the freezer overnight. The mixture was filtered, and the filtrate was evaporated to 10 mL. Cold, deaerated ether (50 mL) was added, and the mixture was chilled in the freezer for 2 h to promote product precipitation. Filtration of the solvent yielded a dark-plum solid in 90% yield (0.2376 g, 0.285 mmol). ^{1}H NMR ($CDCl_3$, ppm): δ 9.92 (1H, s, quin *H*3), 8.21−7.50 (4H, Ar*H*), 5.92 (1H, s, Tp*pyrazolyl-*H*), 5.90 (1H, s, Tp*pyrazolyl-*H*), 5.41 (1H, s, Tp*pyrazolyl-*H*), 2.90 (3H, s, C−CH_3), 2.42 (3H, s, C−CH_3), 2.29 (6H, s, Tp*pyrazolyl-CH_3), 2.28 (3H, s, Tp*pyrazolyl-CH_3), 2.22 (3H, s, Tp*pyrazolyl-CH_3), 2.18 (3H, s, Tp*pyrazolyl-CH_3), 2.02 (3H, s, Tp*pyrazolyl-CH_3). IR (KBr disk): ν(B−H) 2520, ν(Mo═S) 496 cm^{-1}. ESI-MS (CH_3CN): *m*/*z* 703.0 ([M$^-$]), 833 ([M + TEA]$^+$), observed as Mo^{5+}, 963 ([M + 2TEA]$^+$), observed as Mo^{4+}. HRESI-MS (M = $C_{28}H_{34}ON_8S_3BMo$: *m*/*z* 703.1171 ([M$^-$]). Calcd for M$^-$: *m*/*z* 703.117032.

*Tp*Mo^{4+}(S)(pyrrolo-S_2BMOQO)* (**2**). A 40 mL portion of ACN was deaerated over activated alumina for 20 min and then transferred to a deaerated Schlenk flask containing TEA[Tp*Mo(S)S_4] (0.217 g, 0.391 mmol) and BMOQO (0.083 g, 0.390 mmol). The reaction was heated to 70 °C for 4 h and then cooled to room temperature before it was placed in the refrigerator overnight. The dark mixture was filtered, and then the filtrate was concentrated under vacuum on the Schlenk line. Deaerated diethyl ether was added to the residue, and the flask was placed in the refrigerator for 2 h. The crude product was isolated by filtration, yielding a shiny black solid (2.41 g, 3.51 mmol). Purification of **2** is done on a short, fast-running silica gel column. Any TEA[Tp*Mo(O)S_4] contaminant elutes first with dichloromethane and then **2** is eluted with 2−5% MeOH/CH_2Cl_2 as a bright-blue band. ^{1}H NMR (ppm): δ 9.62 (1H, s, quin *H*3), 8.21−7.30 (4H, Ar*H*), 6.15 (1H, s, Tp*pyrazolyl-*H*), 6.12 (1H, s, Tp*pyrazolyl-*H*), 5.25 (1H, s, Tp*pyrazolyl-*H*), 3.07 (3H, s, cyclized C−CH_3), 3.05 (3H, s, cyclized C−CH_3), 2.63 (3H, s, Tp*pyrazolyl-CH_3), 2.60 (3H, s, Tp*pyrazolyl-CH_3), 2.18 (3H, s, Tp*pyrazolyl-CH_3), 2.12 (3H, s, Tp*pyrazolyl-CH_3), 2.10 (3H, s, Tp*pyrazolyl-CH_3), 1.74 (3H, s, Tp*pyrazolyl-CH_3). IR (KBr disk): ν(C═O) and ν(C═N) 1541, 1443, 1438, 1412, 1380, 1365, ν(Mo═S) 523 cm^{-1}. ESI$^+$-MS: *m*/*z* 686 ([M$^+$]) as Mo^{5+}. HRESI-MS (M = $C_{28}H_{33}BN_8S_3Mo$): *m*/*z* 686.1126 ([M$^+$]). Calcd for M: *m*/*z* 686.1132.

*TEA[Tp*Mo^{4+}(O)(S_2BMOQO)]* (**3**). **1** (0.2000 g, 0.2401 mmol) and triphenylphosphine (0.0786 g, 0.300 mmol) were stirred under nitrogen in "wet" ACN (~2% H_2O; 30 mL) at room temperature for 1 h. The mixture was then filtered to remove excess triphenylphosphine, and the filtrate was reduced under vacuum to 5 mL. Deaerated ether (40 mL) was added, and the flask was placed in the freezer overnight. The ether was filtered to yield a dark-purple-red solid in 98% yield (0.1920 g, 0.235 mmol). ^{1}H NMR ($CDCl_3$, ppm): δ 9.95 (1H, s, quin *H*3), 8.11−7.43 (4H, Ar*H*), 5.95 (1H, s, Tp*pyrazolyl-*H*), 5.93 (1H, s, Tp*pyrazolyl-*H*), 5.44 (1H, s, Tp*pyrazolyl-*H*), 2.88 (6H, s, C−CH_3), 2.73 (3H, s, Tp*pyrazolyl-CH_3), 2.35 (3H, s, Tp*pyrazolyl-CH_3), 2.30 (6H, s, Tp*pyrazolyl CH_3), 2.16 (3H, s, Tp*pyrazolyl-CH_3), 2.08 (3H, s, Tp*pyrazolyl-CH_3). IR (KBr disk): ν(B−H) 2530, ν(Mo═O) 914 cm^{-1}. ESI-MS (CH_3CN): *m*/*z* 687 ([M]$^-$), 817 ([M + TEA]$^+$), observed as Mo^{5+}, 947 ([M + 2TEA]$^+$), observed as Mo^{4+}. HRESI-MS (M = $C_{28}H_{34}O_2N_8S_2BMo$): *m*/*z* 687.1400 ([M−]). Calcd for M−: *m*/*z* 687.139876.

*Tp*Mo^{4+}(O)(pyrrolo-S_2BMOQO)* (**4**). **2** (0.200 g, 0.291 mmol) was dissolved in 30 mL of ACN. An excess of triphenylphosphine (0.079 g, 0.300 mmol) was added, and the solution stirred for 1 h at room temperature. The solution was then concentrated under vacuum, and ether was added to yield a dark-blue precipitate in 97% crude yield. The product was chromatographed on neutral alumina using 5% methanol/dichloromethane. ^{1}H NMR (ppm): δ 9.52 (1H, s, quin *H*3), 8.22−7.62 (4H, Ar*H*), 6.00 (1H, s, Tp*pyrazolyl-*H*), 5.98 (1H, s, Tp*pyrazolyl-*H*), 5.43 (1H, s, Tp*pyrazolyl-*H*), 2.81 (3H, s, cyclized C−CH_3), 2.79 (3H, s, cyclized C−CH_3), 2.45 (6H, s, Tp*pyrazolyl-CH_3), 2.29 (6H, s, Tp*pyrazolyl-CH_3), 2.21 (3H, s, Tp*pyrazolyl-CH_3), 1.80 (3H, s, Tp*pyrazolyl-CH_3). ^{13}C{H} NMR (ppm): δ 146 (C3), 133 (C7 and C8), 128, 114 (C6 and C9), 108, 107, 106 (3 *C*H-pyrazole), 17, 16 (−CH_3, BMOQO), 13, 12 (6 −CH_3, pyrazole). IR (KBr disk): ν(C═O) and ν(C═N) 1541, 1443, 1438, 1412, 1380, 1365, ν(Mo≡O) 922 cm^{-1}. ESI$^+$-MS: *m*/*z* 670.0 ([M$^+$]), observed as Mo^{5+}. HRESI-MS (M = $C_{28}H_{33}BON_8S_2Mo$): *m*/*z* 670.1383 ([M$^+$]). Calcd for M: *m*/*z* 670.136039.

*[Tp*Mo^{5+}(O)(pyrrolo-S_2BMOQO)]Cl* (**5**). A 0.050 g sample of blue **4** was dissolved in 10 mL of ACN. A 0.5 mL aliquot of 3% hydrogen peroxide was added, and the reaction immediately turned cherry-red. The sample was then washed with a saline solution, resulting in a bright-pink ACN layer and providing the chloride counterion to precipitate the complex. The addition of hexanes resulted in the precipitation of red, microcrystalline **5** in 92% yield. IR (KBr disk): ν(Mo≡O) 935 cm^{-1}. ESI$^+$-MS: *m*/*z* 670.0 ([M$^+$]). HRESI-MS (M = $C_{28}H_{33}BON_8S_2Mo$): *m*/*z* 670.1377 ([M$^+$]). Calcd for M: *m*/*z* 670.136039.

Reactivity Studies. Experiments on the reactivity of complexes **1**−**4** used ESI-MS to monitor the change in the species distribution as the solution environment was varied. Samples were dissolved in either acetontrile or CH_2Cl_2. Studies on the effect of dehydrating agents used microwave-activated 3 Å molecular sieves or alumina.

Electron Paramagnetic Resonance (EPR) Spectroscopy. EPR spectra were collected at X band (9.3 GHz) using a Bruker EMX spectrometer with associated Bruker magnet control electronics and microwave bridges. Low-temperature spectra were collected in dichloromethane, and the temperature was controlled using an Oxford Instruments liquid-helium flow cryostat. Simulations of the EPR spectra were performed using the program *X-Sophe* and the Matlab toolbox *EasySpin*.[31]

Electronic Absorption Spectroscopy. Electronic absorption spectra were collected using a Hitachi U-3501 UV−vis−near-IR dual-beam spectrometer capable of scanning a wavelength region between 185 and 3200 nm. The electronic absorption spectra were measured in a 1-cm-path-length, 100 μL, black-masked, quartz cuvette (Starna Cells, Inc.) equipped with a Teflon stopper. All electronic absorption spectra were collected at room temperature and repeated at regular time intervals to ensure the stability and integrity of the sample in solution.

Raman Spectroscopy. Solid-state resonance Raman (rR) spectra and associated rR excitation profiles were collected using a system comprised of a PI/Acton SpectraPro SP-2556 500 mm focal length imaging spectrograph with a triple-grating turret and a PI/Acton Spec-10:100B back-illuminated 1340 × 100 pixel digital CCD spectroscopy system with a cryogenically cooled camera head. Coherent Innova Ar^+ and Kr^+ ion lasers were used as the excitation sources. Samples were mixed with either NaCl or a NaCl/Na_2SO_4 mixture with Na_2SO_4 as an internal calibrant. rR excitation profiles were plotted using a Kr^+ laser line at 647 nm and Ar^+ laser lines at 458, 488, and 514 nm where all peaks were normalized with respect to the 992 cm^{-1} Na_2SO_4 peak.

Computational Details. Electronic structure and vibrational frequency calculations were performed at the density functional theory (DFT) level of using the *Gaussian 03W* software package (*Gaussian03*, RCG, Inc., Pittsburgh, PA, 2003). All calculations employed the B3LYP

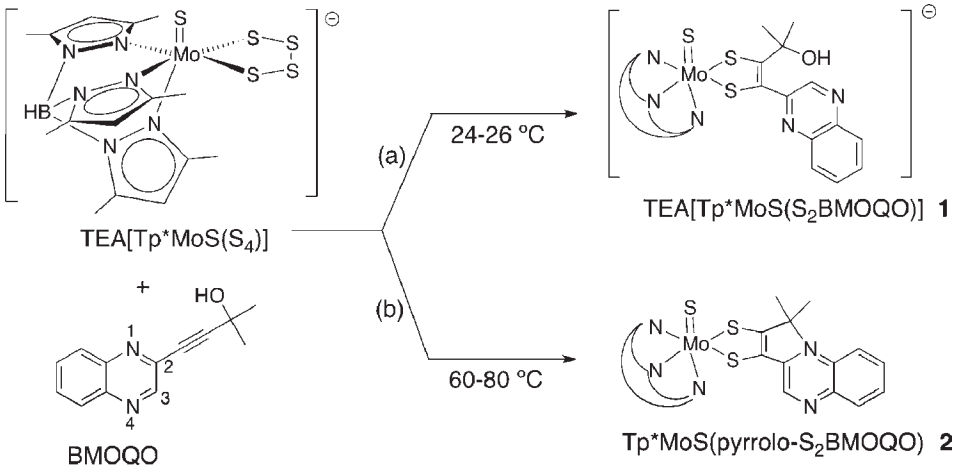

Figure 3. Reaction of molybdenum tetrasulfide and an alkyne (BMOQO) forming a quinoxalyldithiolene complex, **1**, at ambient temperature in path a and a pyrroloquinoxalyldithiolene complex, **2**, under moderate heat in path b.

hybrid functional and used a LANL2DZ basis set with an effective core potential for molybdenum. A 6-31G* basis set was used for all light atoms. Input files were prepared using the molecule builder function in the *Gaussview* software package. The starting geometries were those of complex **4**. All geometries were fully minimized in the calculations. Molecular orbitals were analyzed using the *AOMix* program.[32,33] Electron density difference maps (EDDMs) were constructed using the *GaussSum* suite of programs. EPR parameters were calculated at the DFT level using *ADF2009.01*.[34−42] EPR parameters were calculated at the DFT level using *ORCA 2.7.0*. The ZORA scalar relativistic Hamiltonian with relativistic corrections was incorporated self-consistently in the ORCA calculation.[43]

RESULTS AND ANALYSIS

Synthesis. A coupling reaction between quinoxalylalkyne, BMOQO, and TEA[Tp*Mo(S)(S$_4$)] produces two types of molybdenum quinoxalyldithiolene complexes, where the reaction temperature determines which species forms (Figure 3). The reaction under room temperature conditions results in the formation of **1** containing a 1,2-substituted dithiolene complex (Figure 3a). Elevated reaction temperatures (60−80 °C) cause an intramolecular cyclization that occurs subsequent to dithiolene ligand formation, yielding **2** (Figure 3b).

Complex **2** results from a net loss of the hydroxyl group from the α-C atom of the alkyl side chain on the S$_2$BMOQO dithiolene ligand, followed by intramolecular cyclization, forming a five-membered pyrrole-like ring. A possible mechanism (Figure 4) for the formation of pyrrolodithiolene involves hydroxyl protonation, followed by the loss of water to produce a carbocation on the akyl group. When the quinoxaline group is oriented so that N1 is adjacent to this carbocation, C−N bond formation and intramolecular cyclization result in a pyrrole ring fused to quinoxaline at positions 1 and 2 (Figure 4). The proposed mechanism is supported by the observation that anhydrous conditions, produced by the addition of drying agents like molecular sieves to solutions of **1**, favor the dehydration step and cause rapid cyclization to **2**. The thermal conditions favoring reaction b in Figure 3 likely facilitate quinoxaline rotation, putting N1 in proximity to the carbocation. The removal of water appears to be the key condition favoring cyclization of complex **1** to complex **2**. The oxo analogue of the tetrasulfide reagent, TEA[Tp*Mo(O)(S$_4$)],

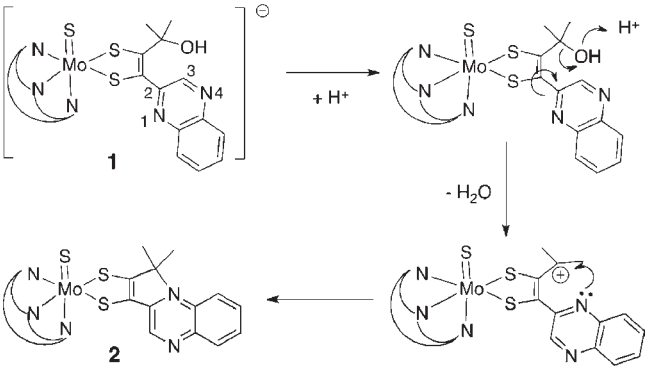

Figure 4. Proposed mechanism for intramolecular cyclization of complex **1**, producing pyrrolodithiolene in **2**.

does not react with alkynes, as was previously reported by us and others.[27,44] Therefore, the use of pure [Tp*Mo(S)(S$_4$)]$^-$ is essential to the isolation of clean sulfido complexes **1** and **2**.

Both sulfido complexes **1** and **2** can be converted to the oxo analogues **3** and **4**, respectively, using triphenylphosphine to faciltate sulfide ligand dissociation. The formation of **3** (eq 1) is best perfomed in "wet" ACN (∼2% H$_2$O) because trace water inhibits the dehydration step in Figure 4 and blocks intramolecular cyclization, which would lead to the pyrroloquinoxalyldithiolene complex **4**.

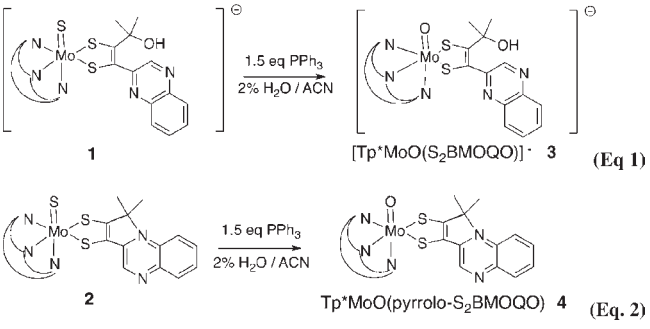

The set of four BMOQO dithiolene complexes **1**−**4** exhibit a range of reactivities. **1** is stable as a solid in both aerobic and anaerobic conditions; however, aerobic dissolution of **1** in a

dx.doi.org/10.1021/ic200783a |*Inorg. Chem.* 2011, 50, 9804–9815

variety of solvents leads to both hydrolysis, forming **3**, and cyclization reactions to yield a mixture of **2** and **4**. The progress of hydrolysis monitored by ESI-MS and ^{1}H NMR indicates that the sulfidodithiolene **1** hydrolyzes to form the oxo complex **3** slowly under anaerobic conditions (several days) when dissolved in ACN containing 2% water (v/v). Because under anaerobic conditions hydrolysis of the sulfido ligand in **1** is relatively slow, the synthesis of **1** can be improved when performed in the presence of trace water because this condition inhibits the dehydration step and pyrrole ring closure while leaving the terminal sulfido ligand intact. The tendency of **1** to dehydrate under anhydrous conditions means that ligand cyclization of **1** to form **2** is accelerated in the presence of molecular sieves. **1** does not survive purification by chromatography because both silica gel and alumina promote the dehydration and formation of **2**, which can be visually identified by its vibrant blue hue. However, this reactivity affords another method to prepare **2** through by column chromatography of **1**, in addition to the thermal reaction (Figure 3b). Plum-red **3** is the least robust of the four molybdenum dithiolenes. The complex is extremely unstable in solution, rapidly cyclizing to **4** within minutes in air, after a few days under a nitrogen atmosphere or by exposure to chromatographic silica or molecular sieves. The deep-blue complex **4** is the most thermodynamically stable member of the four S_2BMOQO dithiolene complexes, and **1**−**3** all ultimately hydrolyze and cyclize to form **4**. The most direct and high-yield preparative route to **4** is by the thermal reaction of BMOQO and $[Tp^*Mo(S)(S_4)]^-$ to produce **2**, followed by hydrolysis in the presence of triphenylphosphine (eq 1) and purification by chromatography on silica. We previously reported how **4** is oxidized by ferrocenium or hydrogen peroxide to the molybdenum(5+) complex **5**.[16] The reaction is a striking one to observe visually because the intensely blue solution of **4** becomes bright cherry red upon the addition of oxidant as the molybdenum(5+) complex **5** forms. Solutions of **5** are not stable, and they slowly revert to the molybdenum(4+) complex, as indicated by a color change to blue. Likewise, **5** cannot be chromatographed because it immediately turns blue on either a silica or alumna support, again indicating a return to the Mo^{4+} oxidation. The greater stability of the Mo^{4+} versus Mo^{5+} state is unique to the presence of the pyrroloquinoxaline dithiolene ligand. All other known dithiolene complexes coordinated to the Tp*Mo(O) unit are isolated in the Mo^{5+} state.

^{1}H and ^{13}C NMR Spectroscopy. ^{1}H NMR spectral data were obtained for all four dithiolene complexes **1**−**4**, confirming the diamagnetic character of the Mo^{4+} formal oxidation state. The complexity of the ^{1}H NMR spectra is a reflection of the low C_1 symmetry of these complexes. Those protons most useful for distinguishing among the four complexes are quinoxaline H3 and the pyrazole ring protons. Quinoxaline H3 appears as a singlet far downfield, remote from all other protons, and is a useful diagnostic of the cyclized or noncyclized state of the dithiolene. The two complexes with "open" dithiolene ligands, **1** and **3**, exhibit H3 downfield at 9.92 and 9.95 ppm, a shift of >1 ppm from H3 in the parent alkyne BMOQO (8.88 ppm). For **2** and **4** having pyrrolodithiolene ligands, H3 appears at 9.62 and 9.52 ppm. The absence of symmetry in the four complexes makes each pyrazolyl ring proton unique in the spectral region 5−6 ppm; however, all four complexes share a pattern where two of the three pyrazolyl protons have chemical shifts near ∼5.9 ppm and one proton occurs at a higher field resonance near 5.4 ppm. This pattern likely reflects the similar environment of the two pyrazole rings that flank dithiolene and the unique environment of the pyrazole ring trans to Mo═X. ^{13}C NMR spectra were obtained only for **4** because of the limited solution stability of complexes **1**−**3**. Assignments for the C atoms in **4** were made by a comparison to reported data for related quinoxaline molecules.[45]

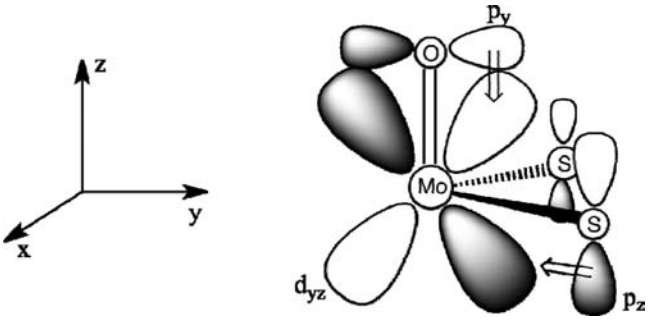

Figure 5. Competition for π donation from oxo and dithiolene orbitals to the Mo d_{yz} orbital.

Vibrational Spectroscopy. Vibrational spectroscopy is a useful tool for the identification of Mo≡X (X = S, O) groups and monitoring of the electronic environment at molybdenum because these vibrational markers correlate with a change in the formal oxidation state of the molybdenum center. Mo≡O stretching frequencies are related to the strength of the π-donor ability of the dithiolene ligand mediated by the S donor atoms. Electron-rich dithiolene ligands donate electron density via their S donor atoms into vacant Mo dπ orbitals (e.g., d_{yz} in Figure 5). This π donation is in competition with the π donation from the terminal oxo ligand and results in lower ν(Mo≡O) stretching frequencies with increased S → Mo charge donation. Conversely, electron-withdrawing substituents on dithiolenes result in increased ν(Mo≡O) stretching frequencies because of poorer S → Mo charge donation. Although the Mo $d_{x^2-y^2}$ orbital is nonbonding with respect to the terminal oxo donor (see Figure 5), dithiolene → Mo $d_{x^2-y^2}$ charge donation leads to a reduction of the metal effective nuclear charge for d^0 Mo^{6+} and d^1 M^{5+} complexes. This, in turn, leads to a decrease in the ionic character of the Mo≡O bond and a corresponding decrease in ν(Mo≡O) stretching frequencies. Molybdenum(4+) monooxo complexes possess a d^2 electron configuration, with the $d_{x^2-y^2}$ orbital being doubly occupied, and this results in no net charge transfer (CT) between dithiolene and the Mo $d_{x^2-y^2}$ orbital.[46] The correlation between the ν(Mo≡O) energy and the electronic character of the ligands on the complex has been studied extensively.[47−49]

Table 1 lists data illustrating these trends for complexes **1**−**5** reported in this work in comparison to data from related Tp*Mo(═X) dithiolene compounds. The Mo═O and Mo═S stretching frequencies observed for complexes **1**−**5** are consistent with those observed in previously reported pterin dithiolene complexes and other Tp*Mo(═X) (X = O, S) dithiolene complexes where, generally, the ν(Mo═X) frequency shifts to higher energy upon oxidation of Mo^{4+} to Mo^{5+}.

A comparison between the Mo≡X (X = O, S) complexes **1**−**5** and the recently reported pterin dithiolenes[27] TEA$[Tp^*Mo^{4+}(X)(S_2DIFPEPP)]$ and $Tp^*Mo^{5+}(X)(S_2DIFPEPP)$ [S_2DIFPEPP = 1,2-(2,4-difluorophenyl)(pterinyl)dithiolene] illustrates the electronic effects of the dithiolene ligands on Mo≡O and Mo≡S stretching frequencies. For oxomolybdenum complexes of both pyrrolo-S_2BMOQO and S_2DIFPEPP dithiolenes, the Mo≡O stretching frequency shifts 13 and 7 cm^{-1}, respectively, to higher energy as the formal molybdenum oxidation state increases from

Table 1. IR Data for 1−5 and Related Tp*Mo(=X) Dithiolene Complexes[a]

	ν(Mo=X), cm^{-1}	ν(BH), cm^{-1}
Compounds Reported in This Work		
TEA[Tp*Mo(S)(S_2BMOQO)] (**1**)	Mo^{4+}=S; 496	2520
Tp*Mo(S)(pyrrolo-S_2BMOQO) (**2**)	Mo^{4+}=S; 523	2542
TEA[Tp*Mo(O)(S_2BMOQO)] (**3**)	Mo^{4+}=O; 914	2530
Tp*Mo(O)(pyrrolo-S_2BMOQO) (**4**)	Mo^{4+}=O; 922	2538
[Tp*Mo(O)(pyrrolo-S_2BMOQO)]Cl (**5**)	Mo^{5+}=O; 935	2545
Related Compounds		
TEA[Tp*Mo(S)(S_2DIFPEPP)][27]	Mo^{4+}=S; 484	2522
Tp*Mo(S)(S_2DIFPEPP)[27]	Mo^{5+}=S; 493	2545
TEA[Tp*Mo(O)(S_2DIFPEPP)][27]	Mo^{4+}=O; 922	2522
Tp*Mo(O)(S_2DIFPEPP)[27]	Mo^{5+}=O; 929	2545
Tp*Mo(S)(S_2DMAC)[44]	Mo^{5+}=S; 490	not reported
Tp*Mo(O)(S_2DMAC)[44]	Mo^{5+}=O; 935	2563
Tp*Mo(O)(tdt)[49]	Mo^{5+}=O; 926	not reported
Tp*Mo(O)(bdt)[49]	Mo^{5+}=O; 932	not reported
Tp*Mo(O)(qdt)[49]	Mo^{5+}=O; 940	2551

[a] DIFPEPP is 1,2-(2,4-difluorophenyl)(pterinyl)dithiolene, DMAC is dimethylcarboxyacetylene, bdt is 1,2-benzenedithiolate, tdt is toluenedithiolate, and qdt is 2,3-quinoxalinedithiolate.

4+ to 5+. The effect of dithiolene substituents on ν(Mo≡O) can be evaluated by comparing data for S_2BMOQO complexes **3** and **4** with those for TEA[Tp*Mo^{4+}(O)(S_2DIFPEPP)].

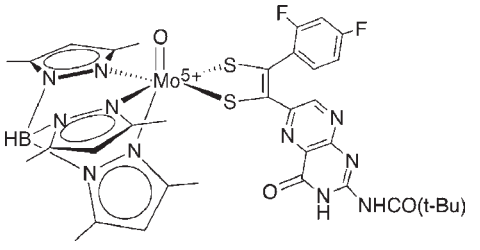

Tp*MoO(S_2DIFPEPP)

A comparison of ν(Mo≡S) in **1** and **2** and ν(Mo≡O) in **3** and **4** indicates that cyclization of the S_2BMOQO ligand to pyrrolo-S_2BMOQO causes an increase in ν(Mo≡S) and ν(Mo≡O) of 27 and 8 cm^{-1}, respectively, due to the electron-withdrawing effect of the conjugated pyrrolo-S_2BMOQO.

The B−H stretching vibration from the Tp* ligand is also a reporter of the electronic change or oxidation state at molybdenum. The data in Table 1 show that ν(BH) shifts to higher energy by as much as 20 cm^{-1} upon oxidation of molybdenum from 4+ to 5+. The electron-withdrawing effect of pyrrolodithiolene in **2** and **4** causes a considerably smaller increase in ν(BH) of 6 and 8 cm^{-1}, respectively, when compared to the "open" dithiolene complexes **1** and **3**.

EPR Spectroscopy of 5. Complex **5** can be readily obtained by hydrogen peroxide or iodine oxidation of **4** to yield the paramagnetic molybdenum(V) species. Room temperature and 75 K EPR spectra for **5** are presented in Figure 6. A simulation of the isotropic spectrum yielded g_{iso} = 1.967 and A_{iso} = 36.80 × 10^{-4} cm^{-1}. Spectral simulation of the anisotropic 75 K data yielded tentative spin Hamiltonian paramters g_1 = 1.997, g_2 = 1.969, and

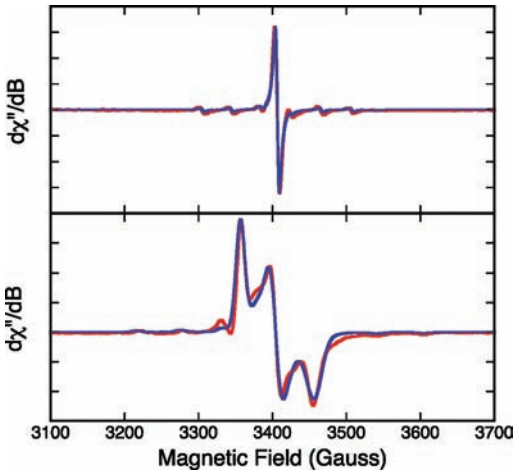

Figure 6. Top: Room temperature solution isotropic EPR spectrum of **5**. Bottom: 75 K EPR spectrum of **5**. All data were collected in CH_2Cl_2.

g_3 = 1.939 (g_{ave} = 1.968) and A_1 = 18 × 10^{-4} cm^{-1}, A_2 = 20 × 10^{-4} cm^{-1}, and A_3 = 62 × 10^{-4} cm^{-1} (A_{ave} = 33 × 10^{-4} cm^{-1}).

The analysis indicates that g_2 and A_2 are essentially coincident and lie near the molecular x axis, while g_1, g_3, A_1, and A_3 are roughly located in the molecular $y-z$ plane, with A_3 oriented very close to the Mo≡O bond. These values are typical of those found for neutral Tp*Mo^{V}O(dithiolene) compounds and compare quite favorably with the spin Hamiltonian parameters that we, and others,[50] have obtained for Tp*MoO(bdt) (bdt = benzene-1,2-dithiolate) g_1 = 2.004, g_2 = 1.972, and g_3 = 1.934 (g_{ave} = 1.970) and A_1 = 60 × 10^{-4} cm^{-1}, A_2 = 26 × 10^{-4} cm^{-1}, and A_3 = 24 × 10^{-4} cm^{-1} (A_{ave} = 37 × 10^{-4} cm^{-1}). The only appreciable difference is an apparent greater rotation of g_1 and g_3 off of A_1 and A_3 in **5**. We note in C_s Tp*MoO(bdt), which possesses a $y-z$ mirror plane, that one component of the **g** tensor and one component of the **A** tensor (e.g., g_2 and A_2) are required to be coincident by symmetry. These results indicate that, for Tp* dithiolene systems, EPR spectroscopy does not appear to be a particularly sensitive probe of the overall complex charge (i.e., cationic vs neutral), the charge on dithiolene, or Mo−$S_{dithiolene}$ bond asymmetry, as found in **5**.

Electronic Absorption Spectroscopy. A striking color change occurs upon cyclization of the open quinoxalyldithiolene ligands in complexes **1** and **3** to the cyclized pyrrolodithiolenes in **2** and **4**. Solutions of complexes **1** and **3** are both red-hued in color, while pyrrolodithiolene complexes **2** and **4** are bright blue. In addition, **4** is solvatochromic and its low-energy absorption undergoes bathochromic shifts of up to 55 nm. The rapid hydrolysis and cyclization reactions of **1** in solution have prevented acquisition of its electronic spectrum. The electronic absorption spectrum of **3** was obtained anaerobically in the presence of wet ACN (2% H_2O) to prevent dithiolene cyclization and is presented in Figure 7. Complex **3** displays an absorption band at 500 nm (20 000 cm^{-1}) responsible for its red color and an intense higher-energy absorption at 320 nm (31 250 cm^{-1}).

Both pyrrolodithiolene complexes **2** and **4** in ACN are intensely blue because of strong abosorptions near 600 nm (~16 400 cm^{-1}). Figure 8 shows the spectrum of **2** (black line) and a spectrum of **4** (red line) generated in situ by hydrolysis of **2**. Remarkably, the 600 nm absorption band of **2** appears to display a vibronic structure in solution with an apparent 1250 cm^{-1} progression. On replacement of the sulfido ligand by an oxo

dx.doi.org/10.1021/ic200783a |Inorg. Chem. 2011, 50, 9804–9815

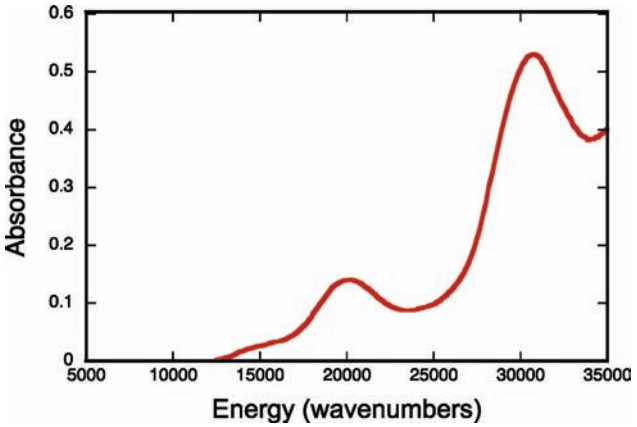

Figure 7. Electronic spectrum of **3** in ACN with 2% H_2O.

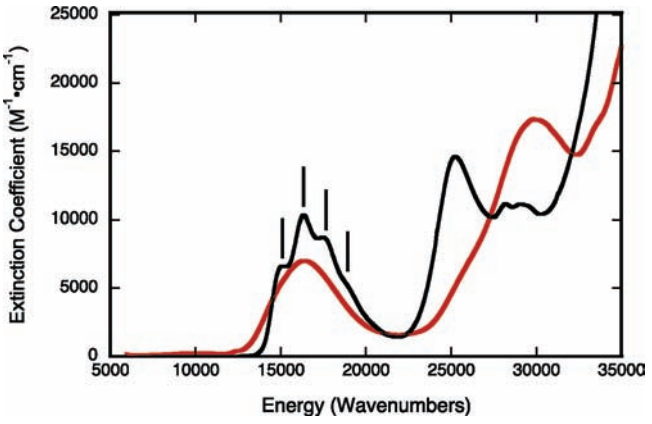

Figure 8. Electronic spectra of **2** (black line) and **4** (red line) in ACN. **2** was hydrolyzed to **4** in dichloromethane. Note the apparent vibronic progression (black sticks) built upon the intense visible band of compound **4** with an apparent progression frequency of 1250 cm^{-1}.

ligand, there is a large hypsochromic shift of 54 nm in the intense high-energy absorption region of the spectrum (from 400 to 346 nm), while the low-energy (~600 nm) absorption envelop of **2** displays a slight decrease in the absorption intensity. We have previously reported the significance of the energy and intensity of the transition associated with the ~600 nm absorption of **4**, and this transition has been assigned as an $S_{dithiolene} \rightarrow$ quinoxaline intraligand CT (ILCT) transition.[28] Because **2** exhibits the same ~600 nm absorption feature as **4**, we also assign this band in **2** as an $S_{dithiolene} \rightarrow$ quinoxaline ILCT transition. This assignment is corroborated by the results of time-dependent DFT calculations, and the intraligand nature of this transition in **2** is clearly evident in the calculated EDDM shown in Figure 9. The assignment of the ~600 nm band in **2** can now be used to understand the electronic origin of the apparent vibronic structure observed for this band. rR spectroscopy identified a number of high-frequency quinoxaline vibrational modes in **4** that were strongly resonantly enhanced with excitation into the 16 400 cm^{-1} ILCT band. Most notable were resonantly enhanced intraligand vibrations that possessed dominant quinoxaline character (1345 cm^{-1}) and C═C plus quinoxaline character (1551 cm^{-1}). The ground-state 1345 cm^{-1} in-plane quinoxaline stretch in **4** correlates very well with the 1250 cm^{-1} excited-state vibration in **2**, when one allows for an ~7% reduction in the ground-state vibrational

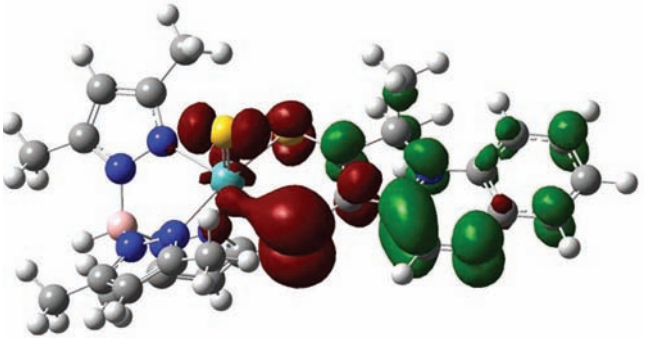

Figure 9. Calculated EDDM that details the nature of the intraligand transition in **2** (red, electron density loss in transition; green, electron density gain in transition).

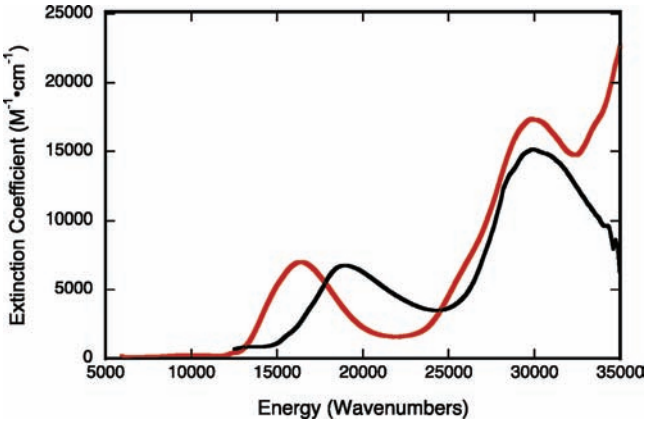

Figure 10. Electronic spectra of **4** (red line) and **5** (black line) in ACN.

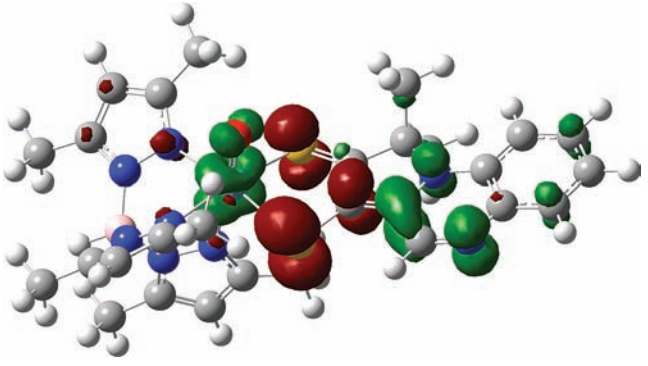

Figure 11. Calculated EDDM that details the nature of the intraligand transition in **5** (red, electron density loss in transition; green, electron density gain in transition.

frequency. Low-temperature studies are planned to further address this issue.

The oxidation of **4** to **5** results in a shift of the ILCT band to higher energies (from 610 to 528 nm), while the UV absorption at 340 nm remains essentially unchanged (Figure 10). The oxidation of **4** does not seem to dramatically affect the nature of the ILCT band, as observed in the calculated EDDM of **5** (Figure 11). However, the ~2500 cm^{-1} increase in the energy of an intraligand transition upon oxidation of the metal ion deserves comment. It is well-known that oxomolybdenum monodithiolenes

dx.doi.org/10.1021/ic200783a |*Inorg. Chem.* 2011, 50, 9804–9815

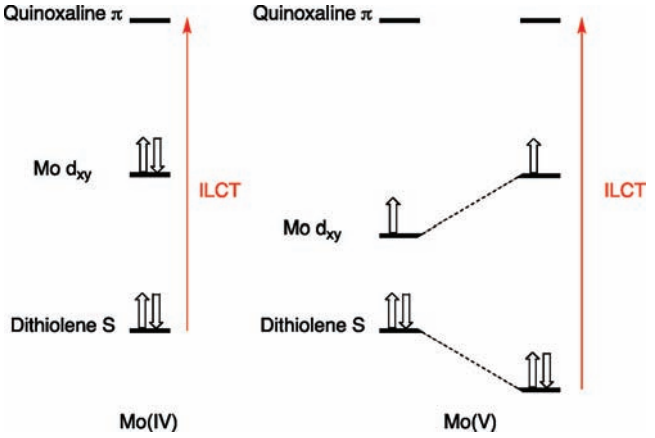

Figure 12. Qualitative energy level diagram showing how fold angle induced dithiolene S-$d_{x^2-y^2}$ interactions in the Mo^{5+} state can stabilize the dithiolene S donor orbitals and result in a higher-energy ILCT band in **5** compared with **4**. The $d_{x^2-y^2}$ orbital is stabilized in Mo^{5+} relative to Mo^{4+} due to the increased valence ionization energy that results from the increased effective nuclear charge due to the metal oxidation. Coupled with the hole created in the Mo $d_{x^2-y^2}$ orbital upon oxidation, the reduced energy gap results in a larger interaction between the Mo^{5+} metal and dithiolene ligand orbitals, and a concomitant increase in dithiolene folding.

undergo an increase in the folding of the dithiolene ligand with an increase in the oxidation state.[51] The hole created in the Mo $d_{x^2-y^2}$ orbital upon one-electron oxidation of the corresponding molybdenum(4+) complex results in increased $S_{dithiolene} \rightarrow$ Mo $d_{x^2-y^2}$ charge donation that is facilitated by folding of the dithiolene ligand about the S---S vector (envelope fold). This has the effect of *stabilizing* the highest occupied dithiolene S orbital that is the donor orbital involved in the $S_{dithiolene} \rightarrow$ quinoxaline ILCT transition and *destabilizing* the Mo $d_{x^2-y^2}$ orbital. The net result is an energetic stabilization of the distorted (i.e., folded) molybdenum(5+) structure over the nondistorted structure and a higher energy $S_{dithiolene} \rightarrow$ quinoxaline CT transition energy in oxidized **5** relative to reduced **4** (Figure 12).

The solution stability of **4** and its solubility in solvents across a broad range of polarity permitted an investigation of its solvatochromic behavior. The low-energy absorption of **4** occurs within the range 596−653 nm, where, in solvents of high dielectric constant, the absorption envelope is centered at higher energies (~600 nm), while low dielectric solvents shift the absorption envelope to ~650 nm (Table 2). These observations are consistent with negative solvatochromic behavior for molecules having a polar ground state and nonpolar excited state. A plot of absorption energy versus Lee's solvent polarity constant E^*_{MLCT} has been shown to yield linear plots for metal-to-ligand CT (MLCT) in various types of complexes.[52] The fact that we observe a nonlinear plot of the data in Table 3 may be interpreted as being consistent with the ILCT assignment for this low-energy transition. Cummings and Eisenberg developed empirical solvent parameters[12] suitable for ligand-to-ligand CT, and the use of these parameters (available for only the four solvents chloroform, acetone, toluene, and DMSO) produced a plot of the solvent parameter versus energy that had a higher linearity.

Cyclic Voltammetry (CV). Three S_2BMOQO dithiolene complexes, **2**−**4**, were studied using CV to compare their $Mo^{5+/4+}$ reduction potentials to those from other members of the Tp*Mo(X)(dithiolene) family. The data in Table 4 are referenced to the ferrocenium/ferrocene couple, whereas the voltammograms in

Table 2. Electronic Spectral Data for Oxo- and Sulfidomolybdenum Dithiolene Compounds

dithiolene complex	λ, nm (ε, M^{-1} cm^{-1})
$[Tp^*Mo(O)(S_2BMOQO)]^-$ (**3**)	~340, ~490
$Tp^*Mo^{4+}(O)$(pyrrolo-S_2BMOQO) (**4**)	336 (13 150), 610 (5190), 1024 (250)
$Tp^*Mo(S)$(pyrrolo-S_2BMOQO) (**2**)	390 (11 765), 527 (5089), 566 (8598), 606 (10 120), 661 (6612)
$[Tp^*Mo^{5+}(O)$(pyrrolo-S_2BMOQO)$]^+$ (**5**)	335 (15 143), 528 (6582)
$Tp^*Mo^{5+}O(S_2DMAC)$	437 (2850), 590 (708), 1125 (385)
$Tp^*Mo^{5+}(O)$(tdt)	403 (5491), 510 (1324), 767 (274), 1100 (490)
$Tp^*Mo^{5+}(O)$(qdt)	389 (4027), 523 (1050), 729 (130), 885 (170)

Table 3. Comparison of the Solvent Polarity and Wavelength in Increasingly Polar Solutions of 4

solvent	Abs_{max}, nm	dielectric constant, ε	E^*_{MLCT}[52]	solvent parameter[12]
toluene	653	2.38	0.30	0.172
diethyl ether	648	4.33	0.32	
chloroform	615	4.81	0.42	0.61
acetone	600	20.7	0.82	0.797
ethanol	600	24.5	0.69	
methanol	596	32.7	0.73	
DMSO	596	46.7	1.00	0.973

Figure 13 are plotted versus the potential of the reference electrode AgCl/Ag. The most stable member of this set, **4**, will be discussed first. The voltammogram of **4** displays two reversible redox couples (Figure 13, top) that have been assigned to the $Mo^{5+/4+}$ (−0.15 V) and pyrrolo-S_2BMOQO ligand reduction events (−1.25 V) based on a comparison to related complexes (see below). In contrast, the "open" dithiolene complex **3** displays a single reversible couple assigned to the $Mo^{4+/5+}$ couple (Figure 6, bottom) and lacks additional redox processes at negative potentials over the same potential window. The voltammogram of **3** shows two small couples (marked with asterisks) at potentials characteristic of **4**, and these provide additional evidence for the solution instability of **3** toward dehydration and intramolecular cyclization during the CV experiment.

The lack of a second reduction process indicates that the "open", noncyclized dithiolene ligand in **3** exhibits no ligand-based redox events in contrast to the redox-active and reducible pyrrolodithiolene ligand in **4**. The $Mo^{4+/5+}$ couple in **3** is ~200 mV more negative than that in **4**, which implies that the pyrrolodithiolene ligand stabilizes Mo^{4+}, a hypothesis consistent with it having appreciable electron-withdrawing character. The sulfidopyrrolodithiolene complex **2** also exhibits both $Mo^{5+/4+}$ and a ligand-based redox process, and these two redox events occur at potentials more negative than those for the oxo complex **4**. The $Mo^{5+/4+}$ potential is 200 mV more negative in the sulfido complex **2** than in the oxo complex **4**, while the pyrrolodithiolene ligand reduction is 330 mV more negative in **2** versus **4**.

The $Mo^{4+/5+}$ redox potentials of the S_2BMOQO dithiolene complexes are compared to those from other Tp*MoX(dithiolene)

dx.doi.org/10.1021/ic200783a |*Inorg. Chem.* 2011, 50, 9804–9815

Table 4. Electrochemical Data for Oxo- and Sulfidomolybdenum Quinoxalyl- and Pterinyldithiolene compounds[a]

dithiolene compound	$E(Mo^{5/4})$, V	ΔE_{pp}, V	i_a/i_c	E(L), V	ΔE_{pp}, V	i_a/i_c
$[Tp^*Mo(O)(S_2BMOQO)]^-$ (**3**)	−0.43					
$Tp^*Mo(O)$(pyrrolo-S_2BMOQO) (**4**)	−0.15	60	0.99	−1.25	62	0.85
$Tp^*Mo(S)$(pyrrolo-S_2BMOQO) (**2**)	−0.35	55	0.59	−1.58	62	0.88
$Tp^*MoO(S_2DIFPEPP)$[27]	−0.44	70	0.93			
$Tp^*MoS(S_2DIFPEPP)$[27]	−0.58	60	0.97			
$Tp^*MoO(S_2PEPP)$[27]	−0.43	68	1.0			
$Tp^*MoS(S_2PEPP)$[27]	−0.59	78	1.0			

[a] All potentials referenced to internal ferrocene whose potential is +0.40 vs the Ag/AgCl reference electrode. ACN = acetonitrile, S_2DIFPEPP = 1,2-(2,4-difluorophenyl)(pterinyl)dithiolene, and S_2PEPP = 1,2-(phenyl)(pterinyl)dithiolene.

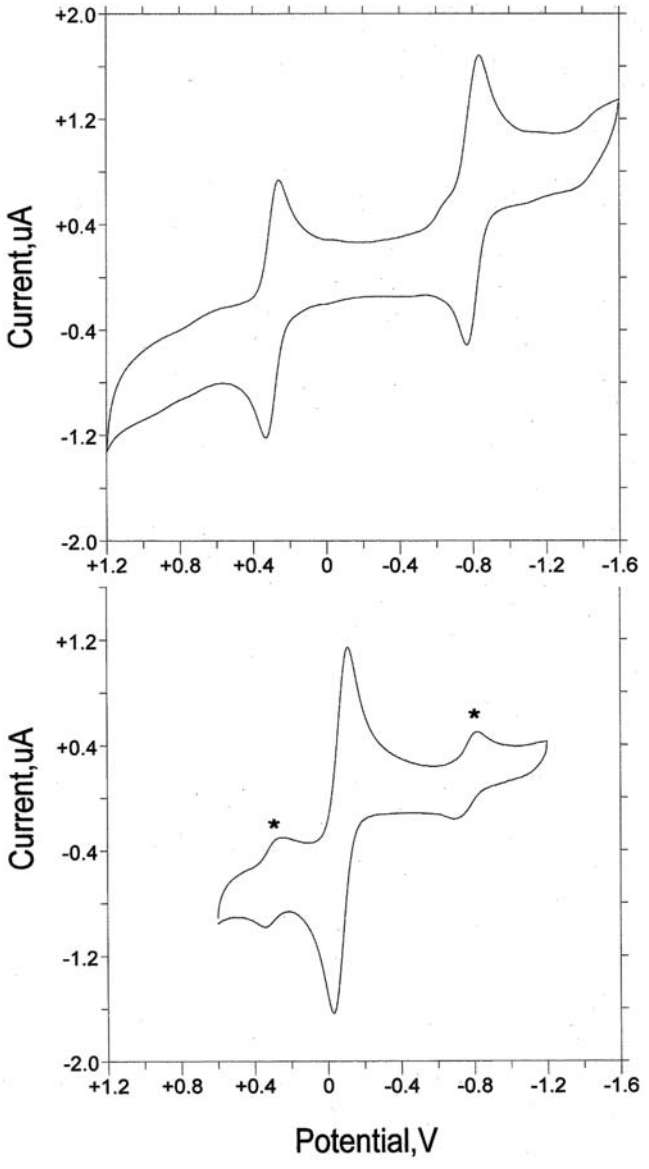

Figure 13. (Top) Cyclic voltammogram of **4**. (Bottom) Cyclic voltammogram of **3**, where the asterisks label the signal due to complex **4** formed during the voltammetry experiment. The voltammograms are plotted versus the potential of reference electrode Ag/AgCl in tetraethylammonium perchlorate/ACN.

compounds in Table 4 and Figure 14. Table 4 compares data for **2**−**4** with data reported from pterin dithiolene complexes of $Tp^*Mo(S,O)$. The $Mo^{5+/4+}$ potential is nearly identical for **3** and the pterin dithiolene compounds, indicating that, from an electronic structure point of view, there is little difference between a quinoxaline and a pterin substituent on a dithiolene ligand coordinated to molybdenum. Oxomolybdenum complexes **3** and **4** are compared to a broader range of $Tp^*Mo(O)$(dithiolene) compounds in Figure 14, where the $Mo^{5+/4+}$ potential is plotted on an electrochemical "yardstick". Several striking points can be made from Figure 14. First, the $Mo^{5+/4+}$ potential spans a range of more than 1 V, where the benzenedithiolate complex $Tp^*MoO(bdt)$ has the most negative value and the pyrrolodithiolene complex **4** has the most positive $Mo^{5+/4+}$ potential. Second, the electronic effect of the pyrrolodithiolene ligand in **4** can be ascertained as more electron-withdrawing than dimethylcarboxalatedithiolene (dmac), which is generally regarded as a very highly electron-deficient dithiolene.[15] However, it should be noted that, in comparison to the anionic complex **3**, complex **4** is a neutral species and would be expected to have a favorable charge effect on the reduction potential that contributes to a more stable reduced form of the $Mo^{5+/4+}$ couple.

DISCUSSION

Five molybdenum dithiolene complexes, TEA[$Tp^*Mo(S)(S_2BMOQO)$] (**1**), $Tp^*Mo(S)$(pyrrolo-S_2BMOQO) (**2**), TEA[$Tp^*Mo(O)(S_2BMOQO)$] (**3**), $Tp^*Mo(O)$(pyrrolo-S_2BMOQO) (**4**), and $[Tp^*Mo(O)$(pyrrolo-S_2BMOQO)$]^+$ (**5**), have been synthesized and characterized. The dithiolene ligand is generated during the synthesis of **1** by a coupling reaction of quinoxalylalkyne with a molybdenum tetrasulfide reagent, [TEA][$Tp^*Mo(S)(S_4)$]. Complexes **1**−**3** are prone to two types of ligand-based reactions: (1) hydrolysis of the Mo═S unit in **1** and **2** to form the corresponding Mo≡O unit in **3** and **4** and (2) pyrrole ring formation following loss of the side chain hydroxyl group as water in **1** and **3** to yield **2** and **4**. Both of these reactions occur during chromatographic purification. During synthesis, however, the dehydration that precedes facile pyrrole ring closure can be controlled by adjusting the reaction environment. For example, the addition of 1−2% water to the reaction solvent prevents dehydration and pyrrole ring closure to favor formation of **1** and **3**, whereas the addition of molecular sieves removes water and favors pyrrole ring formation to yield **2** and **4**. Surprisingly, the Mo≡S group persists under conditions of trace water and is not hydrolyzed during the course of the reaction, indicating that the side-chain hydroxyl is a more reactive site than the sulfido ligand with respect to hydrolysis. The irreversible nature of these two ligand reactions requires that the reaction and isolation conditions for **1**−**3** be carefully monitored to avoid their conversion to the most stable member of this set, **4**.

dx.doi.org/10.1021/ic200783a |*Inorg. Chem.* 2011, 50, 9804–9815

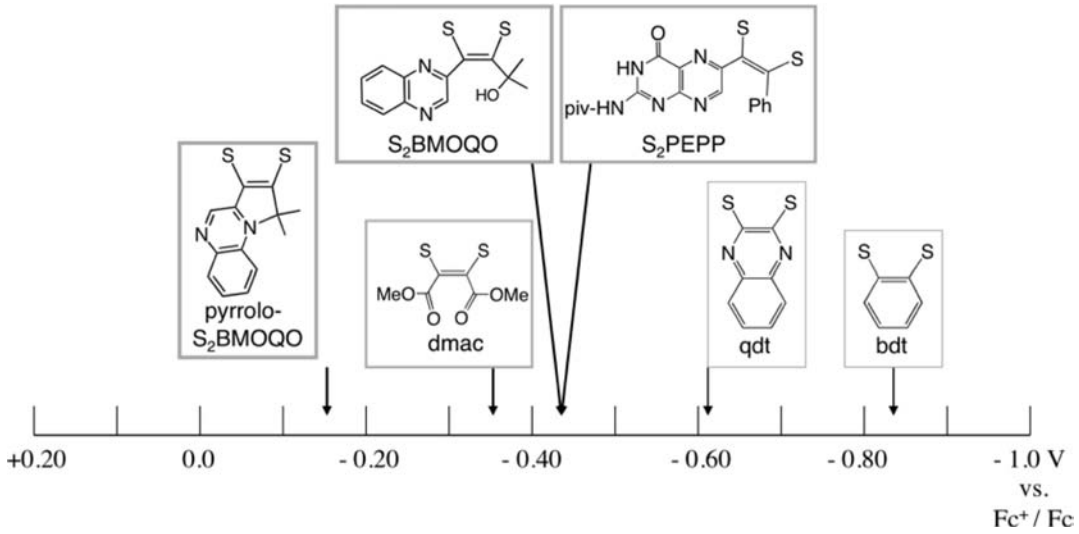

Figure 14. $Mo^{5+/4+}$ reduction potentials for Tp*MoO(dithiolene) complexes in ACN referenced to ferrocenium/ferrocene. Potentials are taken from the literature (dithiolene, $Mo^{5+/4+}$, V: bdt, −0.84;[49] qdt, −0.62;[49] dmac, −0.35;[44] S_2PEPP, −0.44[27]).

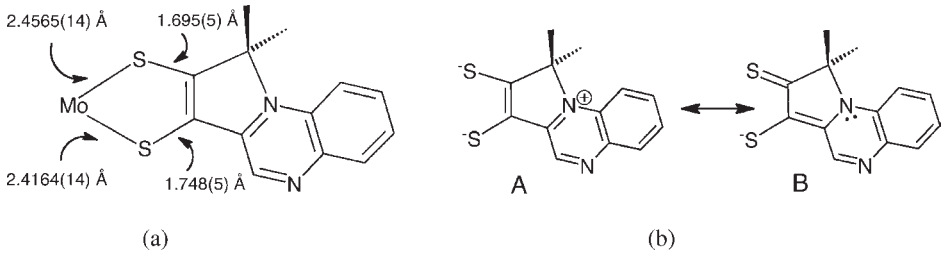

Figure 15. (a) Asymmetry in the bond distances of dithiolene chelate in **4**. (b) Key resonance structures for the asymmetric dithiolene in **4**.

We previously reported that an unusual electronic structure exists in dithiolene complex **4** based on the results from X-ray crystallography, electronic spectroscopy, rR spectroscopy, and DFT calculations.[28] The structure of the dithiolene chelate in **4** is asymmetric (Figure 15a), where the two Mo−S and C−S bond distances differ by ∼0.04 and 0.05 Å, respectively. DFT calculations probing on the ground-state and electronic transitions of **4** produced descriptions of the highest occupied molecular orbital (HOMO) as primarily localized on the dithiolene S atoms and the lowest unoccupied molecular orbital (LUMO) as predominantly quinoxaline-based. This led to an assignment of the intense visible absorption near 600 nm as intraligand dithiolene → quinoxaline CT (ILCT) transition. rR excitation profiles supported this assignment because excitation into the intense 600 nm absorption results in resonantly enhanced quinoxaline vibrations between 1300 and 1500 cm^{-1}.[28] These results led to an interpretation of the electronic structure of molybdenum dithiolene as possessing thiolate−thione character contributed by resonance structure B in Figure 15b. The partial oxidation of a thiolate to a thione illustrated in resonance structure B may be viewed as a consequence of the strong electron-withdrawing effect of the pyrroloquinoxaline structure on the dithiolene. Data reported in this work (IR, CV, and UV−vis) further support this strong electron-withdrawing effect and ILCT assignment. The $Mo^{5+/4+}$ potential for the pyrrolo-S_2BMOQO complex **4** is ∼200 mV more positive than the noncyclized -S_2BMOQO dithiolene complex **3**, and this easier reduction of molybdenum is consistent with the shift of the electron density from the Mo ion to pyrroloquinoxaline mediated by the dithiolene chelate. Indeed, the $Mo^{5+/4+}$ potential in **4** at +250 mV is the most positive redox potential ever found for a Tp*Mo(O)(dithiolene) species and explains the exceptional stability of molybdenum(4+) in the class of Tp*MoO-dithiolenes typically most stable as molybdenum(5+) complexes.

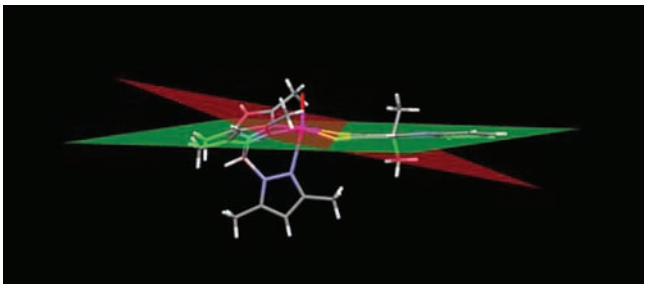

Figure 16. Dihedral fold angle in **4**. The red plane is calculated through the atoms Mo−S1,S2 of the dithiolene chelate, and the green plane is calculated through dithiolene atoms S1, S2, C1, and C2.

The proposed strong electron-withdrawing effect of the asymmetric thione−thiolate ligand is consistent with the dithiolene fold angle of ∼14° in **4** (Figure 16). Dithiolene fold angles, i.e., the dihedral angle between planes formed by the M−S−S and S−C−C−S atoms, have been used as indicators to evaluate the extent of S(π p) → M(d) donation in metal dithiolenes and dithiones.[53−57] Dithiolene and dithione folding increases with an

dx.doi.org/10.1021/ic200783a |*Inorg. Chem.* 2011, 50, 9804–9815

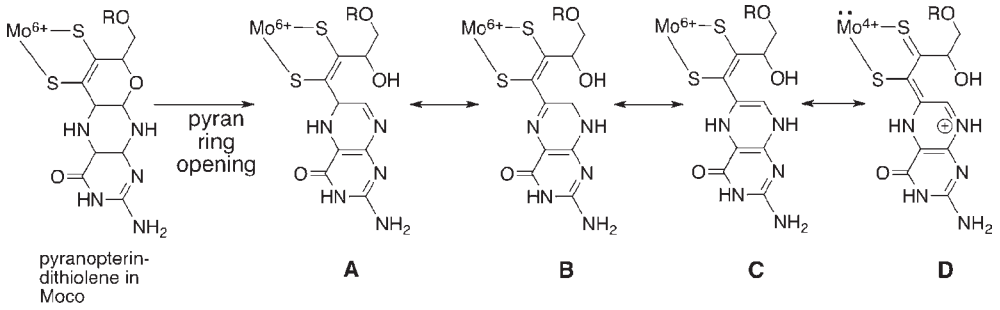

Figure 17. Pyran ring-opening reaction in Moco, which can generate tautomers A−D by proton migration around the pyrazine ring of pterin. Valence tautomer D possesses the thione−thiolate chelate form resulting from a formal two-electron intramolecular redox reaction that produces reduced Mo^{4+} and an oxidized pterin dithiolene ligand.

increase in the oxidation state of the metal as a result of increased S(π p) → M(d) donation.[54,55] The metal ion in **4** is assigned a formal Mo^{4+} oxidation and would be expected to exhibit a dithiolene fold angle near 0°. The observed fold angle of ∼14° in **4** corresponds to an intermediate value in the range observed for complexes of the formal oxidation state Mo^{4+} to Mo^{5+}. We interpret this result as indicative the electronic delocalization between Mo^{4+} ion to the pyrroloquinoxaline dithiolene ligand. Variation of the dithiolene fold angle has been argued to potentially play a role in electronic modulation within the molybdenum pyranopterin dithiolene unit of Moco during catalysis.[53,58]

One other example of ditholene asymmetry in a molybdenum(4+) complex exists where the dithiolene ligand is also substituted by quinoxaline. $(Cp)_2Mo$(quinoxalyldithiolene) (**6**; eq 3) possesses the same pyrrolodithiolene ring system as **2** and **4**, and this dithiolene ligand is formed by a related reaction shown in eq 3. Electrophilic attack by the α-C atom is promoted by acid addition to a ketone precursor (eq 3).[59] A similar thione−thiolate electronic structure for the chelate can be inferred from the asymmetry in the S−C distances [S(1)−C(11) 1.706 Å vs S(2)−C(12) 1.762 Å] and from the intense low-energy absorption (746 nm, 6900 M^{-1} cm^{-1}).

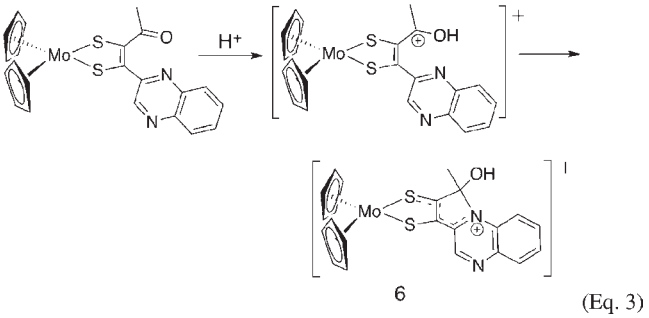

(Eq. 3)

Complexes **1**−**5** reported here provide new information on how N-heterocycles affect the electronic environments of molybdenum dithiolenes. Previous work has shown that protonation of quinoxalines and pyridines increases molybdenum redox potentials and that the basicity of N-cycles is increased (ΔpK_a 1−3 units higher) when N-cycles are subsitutents on dithiolenes chelated to metals.[60] The increased basicity was attributed to resonance stabilization of the N-heterocycle through a contributing thione−thiolate resonance structure, and analogous ILCT [dithiolene (S) → N-heterocycle] transitions were assigned.[60] Here we have described the conditions for a facile and thermodynamically favored intraligand cyclization that illustrates how reactions involving hydroxyalkyl substiuents on quinoxalinedithiolene ligands can be more favored than the reaction at Mo≡S. We have observed similar reactivity on pterin dithiolenes that will be reported later.

These studies provide examples of the roles that the N-heterocycle pterin can play as an essential part of the molybdenum cofactor (Moco). While pyrrole cyclization is not likely to have any role in the cofactor function, the electronic redistribution within the dithiolene chelate that results from electrophilic attack at pyrazine N atom does provide a valuable structural model for the consquence of protonation at pterin N atoms, and this is illustrated in Figure 17. Following pyrano ring opening in Moco, proton migration around the pyrazine ring of the pterin system accesses several different tautomers, A−D, and one of those (D) possesses the asymmetric thione−thiolate chelate. Such a ring-opening reaction of pyranopterin has been documented in several enzymes.[24−26] The rearrangements in Figure 17 present examples of the electronic distribution consequences that may be operative in the enzymes. The results reported here provide evidence for the magnitude of the electronic effect of introducing thione−thiolate character into a dithiolene chelate on the redox potential of molybdenum.

CONCLUSION

The presence of the S_2BMOQO dithiolene ligand in both oxo and relatively rare sulfido complexes of molybdenum(4+) alters the electronic properties of the overall molybdenum dithiolene complex, as shown through comparisons of these compounds to first-generation models such as Tp*Mo(O)(bdt), Tp*Mo(O)(tdt), and Tp*Mo(O)(qdt). This study points to a unique noninnocent ligand. The versatile nature of the BMOQO dithiolene unit may be relevant to the pterin dithiolene ligand found in Moco because it is hypothesized that pyranopterin aids in the modulation of the redox processes of the molybdenum center during the course of enzyme catalysis.

AUTHOR INFORMATION

Corresponding Author

*E-mail: sburgmay@brynmawr.edu (S.J.N.B.), mkirk@unm.edu (M.L.K.).

ACKNOWLEDGMENT

M.L.K. acknowledges the NIH (Grant GM-057378) and the NSF (Grant CHE-0616190) for financial assistance. S.J.N.B. acknowledges the NIH (Grant GM081848). The authors thank Benjamin Stein for helpful discussions.

REFERENCES

(1) Stiefel, E. I.; Eisenberg, R.; Rosenberg, R. C.; Gray, H. B. *J. Am. Chem. Soc.* **1966**, *88*, 2956–2966.
(2) Burgmayer, S. J. N. *Prog. Inorg. Chem.* **2004**, *52*, 491–538.
(3) Basu, P.; Burgmayer, S. J. N. *Coord. Chem. Rev.* **2011**, *255*, 1016–1038.
(4) Kirk, M. L.; Helton, M. E.; McNaughton, R. L. *Prog. Inorg. Chem.* **2004**, *52*, 111–212.
(5) Cassoux, P.; Valade, L.; Kobayashi, H.; Kobayashi, A.; Clark, R. A.; Underhill, A. E. *Coord. Chem. Rev.* **1991**, *110*, 115.
(6) Faulmann, C.; Cassoux, P. *Prog. Inorg. Chem.* **2004**, *52*, 399–490.
(7) Kato, R.; Liu, Y. L.; Aonuma, S.; Sawa, H. *Synth. Met.* **1997**, *86*, 2087.
(8) Tanaka, H.; Okano, Y.; Kobayashi, H.; Suzuki, W.; Kobayashi, A. *Science* **2001**, *291*, 285.
(9) Pilato, R. S.; Van Houten, K. A. *Prog. Inorg. Chem.* **2004**, *52*, 369–397.
(10) Marbella, L.; Serli-Mitasev, B.; Basu, P. *Angew. Chem., Int. Ed.* **2009**, *48*, 3996–3998.
(11) Eisenberg, R.; Gray, H. B. *Inorg. Chem.* **2011**, in press (manuscript in this Forum).
(12) Cummings, S. D.; Eisenberg, R. *J. Am. Chem. Soc.* **1996**, *118*, 1949–1960.
(13) Zuleta, J. A.; Bevilacqua, J. M.; Rehm, J. M.; Eisenberg, R. *J. Am. Chem. Soc.* **1992**, *31*, 1332–1337.
(14) Pierpont, C. *Coord. Chem. Rev.* **2001**, *219*−*221*, 415–433.
(15) Kaufmann, H. L.; Liable-Sands, L.; Rheingold, A. L.; Burgmayer, S. J. N. *Inorg. Chem.* **1999**, *38*, 2592–2599.
(16) Burgmayer, S. J. N.; Arkin, M. R.; Bostick, L.; Dempster, S.; Everett, K. M.; Layton, H. L.; Paul, K. E.; Rogge, C.; Rheingold, A. L. *J. Am. Chem. Soc.* **1995**, *117*, 5812–5823.
(17) Fischer, B.; Straehle, J.; Viscontini, M. *Helv. Chim. Acta* **1991**, *74*, 1544–1554.
(18) Miyazaki, S.; Kojima, T.; Mayer, J. M.; Fukuzumi, S. *J. Am. Chem. Soc.* **2009**, *131*, 11615–11624.
(19) Miyazaki, S.; Kojima, T.; Sakamoto, T.; Matsumoto, T.; Ohkubo, K.; Fukuzumi, S. *Inorg. Chem.* **2007**, *47*, 333–343.
(20) Burgmayer, S. J. N.; Kaufmann, H. L.; Fortunato, G.; Hug, P.; Fischer, B. *Inorg. Chem.* **1999**, *38*, 2607–2613.
(21) Enemark, J. H.; Garner, C. D. *J. Biol. Inorg. Chem.* **1997**, *2*, 817–822.
(22) Burgmayer, S. N. J.; Pearsall, D. L.; Blaney, S. M.; Moore, E. M.; Sauk-Schubert, C. *J. Biol. Inorg. Chem.* **2004**, *9*, 59–66.
(23) Greatbanks, S. P.; Hillier, I. H.; Garner, C. D.; Joule, J. A. *J. Chem. Soc., Perkin Trans.* **1997**, *2*, 1529–1534.
(24) Bertero, M. G.; Rothery, R. A.; Palak, M.; Hou, C.; Lim, D.; Blasco, F.; Weiner, J. H.; Strynadka, N. C. J. *Nat. Struct. Biol.* **2003**, *10*, 681–687.
(25) Jormakka, M.; Richardson, D.; Byrne, B.; Iwata, S. *Structure* **2004**, *12*, 95–104.
(26) Kloer, D. P.; Hagel, C.; Heider, J.; Schultz, G. E. *Structure* **2006**, *14*, 1377–1388.
(27) Burgmayer, S. J. N.; Kim, M.; Petit, R.; Rothkopf, A.; Kim, A.; Bel Hamdounia, S.; Hou, Y.; Somogyi, A.; Habel-Rodriguez, D.; Williams, A.; Kirk, M. L. *J. Inorg. Biochem.* **2007**, *101*, 1601–1616.
(28) Matz, K. G.; Mtei, R. P.; Leung, B.; Burgmayer, S. J. N.; Kirk, M. L. *J. Am. Chem. Soc.* **2010**, *132*, 7830.
(29) Curtis, M. D.; Shiu, K. *Inorg. Chem.* **1985**, *24*, 1213–1218.
(30) Seino, H.; Arai, Y.; Iwata, N.; Nagao, S.; Mizobe, Y.; Hidai, M. *Inorg. Chem.* **2000**, *40*, 1677–1682.
(31) Stoll, S.; Schweiger, A. *J. Magn. Reson.* **2006**, *178*, 42.
(32) Gorelsky, S. I. *AOMix: Program for Molecular Orbital Analysis*; York University: Toronto, 1997; http://www.sh-chem.net/.
(33) Gorelsky, S. I.; Lever, A. B. P. *J. Organomet. Chem.* **2001**, *635*, 187–196.
(34) *ADF2009.01*; SCM, Theoretical Chemistry, Vrije Universiteit: Amsterdam, The Netherlands, 2009; http://www.scm.com.
(35) *Gaussian03*, RCG, Inc.: Pittsburgh, PA, 2003.
(36) Becke, A. *J. Chem. Phys.* **1993**, *98*, 5648.
(37) van Lenthe, E.; van der Avoird, A.; Wormer, P. E. S. *J. Chem. Phys.* **1998**, *108*, 4783.
(38) van Lenthe, E.; Wormer, P. E. S.; van der Avoird, A. *J. Chem. Phys.* **1997**, *107*, 2488.
(39) Neese, F. *ORCA, an ab initio, density functional, and semi-empirical program package*; Version 2.8.0; University of Bonn: Bonn, Germany, 2010.
(40) Neese, F. *J. Chem. Phys.* **2001**, *115*, 11080.
(41) Neese, F. *J. Chem. Phys.* **2003**, *119*, 9428.
(42) Neese, F. *J. Chem. Phys.* **2003**, *118*, 3939.
(43) Cauzzi, D.; Delferro, M.; Graiff, C.; Pattacini, R.; Predieri, G.; Tiripicchio, A. *Coord. Chem. Rev.* **2010**, *254*, 753−764.
(44) Sproules, S. A.; Morgan, H. T.; Doonan, C. J.; White, J. M.; Young, C. G. *Dalton Trans.* **2005**, 3552–3557.
(45) Bradshaw, B.; Collison, D.; Garner, C. D.; Joule, J. A. *Org. Biomol. Chem.* **2003**, *1*, 129.
(46) Bersuker, I. B. *Electronic Sturcture and Properties of Transition Metal Compounds. Introduction to the Theory*; Wiley-Interscience: New York, 1996.
(47) Chang, C. S. J.; Enemark, J. H. *Inorg. Chem.* **1991**, *30*, 683.
(48) Garner, C. D.; Hill, L.; Howlander, N. C.; Hyde, M. R.; Mabbs, F. E.; Routledge, V. I.; Less, J. *Common Mat.* **1977**, *54*, 27.
(49) Helton, M. E.; Gruhn, N. E.; McNaughton, R. L.; Kirk, M. L. *Inorg. Chem.* **2000**, *39*, 2273–2278.
(50) Dhawan, I. K.; Enemark, J. H. *Inorg. Chem.* **1996**, *35*, 4873–4882.
(51) Cooney, J. A. M. A. C.; Gruhn, N. E.; Joshi, H. K.; Enemark, J. H. *Inorg. Chem.* **2004**, *43*, 8110–8118.
(52) Manuta, D. M.; Lees, A. J. *Inorg. Chem.* **1983**, *22*, 3825–3828.
(53) Inscore, F. E.; Knottenbelt, S. Z.; Rubie, N. D.; Joshi, H. K.; Kirk, M. L.; Enemark, J. H. *Inorg. Chem.* **2006**, *45*, 967–976.
(54) Joshi, H. K. F. E. I.; Schirlin, J. T.; Dhawan, I. K.; Carducci, M. D.; Bill, T. G.; Enemark, J. H. *Inorg. Chim. Acta* **2002**, *337*, 275–286.
(55) Joshi, H. K.; Cooney, J. A.; Inscore, F. E.; Gruhn, N. E.; Lichtenberger, D. L.; Enemark, J. H. *Proc. Natl. Acad. Sci. U.S.A.* **2003**, *100*, 3719–3724.
(56) Kapre, R.; Ray, K.; Sylvestre, I.; Weyhermüller, T.; DeBeer George, S.; Neese, F.; Wieghardt, K. *Inorg. Chem.* **2006**, *45*, 3499–3509.
(57) Nemykin, V. N.; Olsen, J. G.; Perera, E.; Basu, P. *Inorg. Chem.* **2006**, *45*, 3557–3568.
(58) Joshi, H. K.; Enemark, J. H. *J. Am. Chem. Soc.* **2004**, *126*, 11784–11785.
(59) Pilato, R. S.; Eriksen, K.; Greaney, M. A.; Gea, Y.; Taylor, E. C.; Goswami, S.; Kilpatrick, L.; Spiro, T. G.; Rheingold, A. L.; Stiefel, E. I. *ACS Symp. Ser.* **1993**, *535*, 83–97.
(60) Hsu, J. K.; Bonangolino, C. J.; Kaiwar, S. P.; Boggs, C. M.; Fettinger, J. C.; Pilato, R. S. *Inorg. Chem.* **1996**, *35*, 4743–4751.